Energy 192 (2020) 116670

Contents lists available at ScienceDirect

Energy

journal homepage: www.elsevier.com/locate/energy

Design and optimization of bio-inspired wave-like channel for a PEM fuel cell applying genetic algorithm

Genchun Cai [b], Yunmin Liang [a], Zhichun Liu [a, b, *], Wei Liu [a]

[a] School of Energy and Power Engineering, Huazhong University of Science and Technology, 430074, Wuhan, China
[b] China-EU Institute for Clean and Renewable Energy at Huazhong University of Science and Technology, 430074, Wuhan, China

ARTICLE INFO

Article history:
Received 12 July 2019
Received in revised form
14 October 2019
Accepted 30 November 2019
Available online 4 December 2019

Keywords:
Proton exchange membrane fuel cell
Bio-inspired wave-like flow channel
Current density
Pressure drop
Genetic algorithm

ABSTRACT

Channel shape design has a significant effect on the performance of a proton exchange membrane fuel cell. Inspired by the fins of cuttlefish, a bio-inspired wave-like structure is designed and applied to the channel of fuel cells. The impact of this bio-inspired wave-like channel on fuel cell performance is investigated through a three-dimensional and non-isothermal model developed in COMSOL Multiphysics. The effects of channel center amplitude and number of wave cycles on the current density and pressure drop of fuel cells are studied. Compared with fuel cells with basic straight channel and conventional wave-like channel, the results show that fuel cell with this bio-inspired wave-like channel has high efficiency and low flow resistance, which can obtain better comprehensive performance. In addition, an optimization of the waveform for bio-inspired wave-like channel is performed by genetic algorithm in consideration of the output power and power consumption of flow. The optimal channel with a center amplitude of 0.305 mm and the number of wave cycles of 3.52 improves the output power density by 2.2%.

1. Introduction

In recent years, to cope with the challenges of energy shortages and climate change, clean and renewable energy has been vigorously developed. Proton exchange membrane fuel cell (PEMFC), an electrochemical converter, is considered as a sustainable power source alternative on account of its high efficiency and environmental friendly characteristics, which has been proven to be attractive in some applications like stationary and portable power systems [1,2]. However, due to its high cost and low durability, PEMFC still faces limitations of a wide commercialization [3]. Optimizing design and enhancing mass transfer to improve the performance and save the cost turn out to be an effective solution. PEMFC is a complex system involving several disciplines so that there are multiple factors affecting its performance. Published reviews show that with mature and reliable computational fluid dynamics (CFD) technologies, PEMFC can be efficient and accurate modeled through different dimensions to investigate the performance of different designs [4–6]. In particular, one important aspect for PEMFC design is geometric structure of channel which plays a significant role in the reactants transportation and distribution.

Extensive researches have been done for the purpose of improving the performance of PEMFC through channel configuration design and parametric study. Recently, Ramin et al. [7] introduced a trap-shape channel design for PEMFCs, and they observed that channels with two 8-mm-long traps can increase the current density and benefit to the distribution of oxygen and water over the cathode catalyst layer (CCL). Yin et al. [8] investigated the characteristics of mass transport and performance of PEMFC with baffle plate installed in the flow channel. The results showed that the baffle plate increases the local gas velocity, which promotes reactants transportation and water removal. Fan et al. [9] proposed two novel PEMFC cathode channel designs (multi-plates structure and integrated structure). Both of them divert more oxygen towards CCL to improve the electrochemical reaction rate, increasing net power density by 4.7% and 7.5%, respectively. Shen et al. [10] studied the performance of a PEMFC with four different blockages in the flow channel and adopted the principle of field synergy based on enhanced mass transfer. They discovered that with blockages, the average synergy angle between the gas velocity and concentration gradient decreases and the effective mass transfer

* Corresponding author. School of Energy and Power Engineering, Huazhong University of Science and Technology, 430074, Wuhan, China.
E-mail address: zcliu@hust.edu.cn (Z. Liu).

https://doi.org/10.1016/j.energy.2019.116670
0360-5442/

Nomenclature

a	water activity
A	area (m^2)
C	molar concentration (mol m^{-3})
C_p	specific heat capacity (J kg^{-1} K^{-1})
D	mass diffusivity (m^2 s^{-1})
E	wavelength (mm)
EW	equivalent molecular weight of electrolyte in membrane (kg mol^{-1})
H	center amplitude (mm)
i	current density (A cm^{-2})
J	volumetric exchange current density (A m^{-3})
k	thermal conductivity (W m^{-1} K^{-1})
K	permeability (m^2)
M	molecular weight (kg mol^{-1})
n_d	electro-osmotic drag coefficient
N	number of wave cycles
p	pressure (atm or Pa)
RH	relative humidity
S	source term
T	temperature (K)
$\mathbf{u}$	velocity (m s^{-1})
V	voltage (V)

Greek letters

α	transfer coefficient
ε	porosity
ζ	stoichiometric ratio
η	overpotential (V)
λ	membrane water content
μ	viscosity (Pa s^{-1})
ρ	density (kg m^{-3})
σ	conductivity (S m^{-1})
ω	species mass fraction
ϕ	potential (V)
ϕ_L	Thiele modulus

Subscripts and Superscripts

0	standard state
a	anode
agg	agglomerate
c	cathode
ch	channel
eff	effective
in	inlet
mem	membrane
ref	reference
sat	saturation
sol	solid phase
w	water

coefficient improves. Mancusi et al. [11] simulated a PEMFC with a tapered channel in different taper angles and temperatures. Their results revealed that the water removal is enhanced owing to airflow velocity increased as tapering the channel downstream. Heidary et al. [12] evaluated the effect of channels with partial or full block in a PEMFC. Due to the blockage, the reactants are forced into the gas diffusion layer (GDL) and the mass transport from the channel to the CCL is facilitated, which in turn improves the cell performance. Besides, compared to partial blockage, full blockage achieves higher net electrical power but also higher pressure drop. Li et al. [13] performed studies on a PEMFC with a periodic waved serpentine flow channel which caused cyclical variation of local flow direction, local flow velocity and local pressure, thus leading to forced-convection enhancement and peak power density increase of 17.8%. Moreover, the channel-rib width is also a vital consideration when design the flow channel for a PEMFC [14–16]. Researches indicated that the channel-rib width has different effects on the cell current density and pressure drop. Meanwhile, overall performance results from a competition between the current collection by the ribs and the oxygen supply from the gas channel to the CCL. There are many other special structure designs applied in different fields for the purpose of improving performance [17,18].

For the optimization of channel geometric structure, numerous researchers have adopted different methodologies and evaluation objectives. Behrou et al. [19] designed the flow field of PEMFCs using topology optimization. The objective is formulated maximize both the output power and homogeneity of current density distribution premising reduced cost. Barati et al. [20] conducted studies on the performance of PEMFCs with pin fins inserted in the flow channel, and optimized the block length, width and hydrogen velocity by respond surface methodology in order to minimize the pressure drop and maximize the total flux magnetic H_2 to GDL. Seyhan et al. [21] adopted artificial neural network to predict the output current of PEMFCs with wavy serpentine flow channels, varying the gas flow rate and amplitude of channel. Specially, genetic algorithm (GA) is confirmed to be one of the significant candidates in optimizing the performance of PEMFCs. Tahmasbi et al. [22] utilized GA and Pareto set to find an optimization model of the PEMFC system based on simultaneous power maximization and cost minimization. Yang et al. [23] applied GA to conduct a channel geometry optimization by vary the channel and rib widths. They studied two types of channel and rib arrangement: symmetric and reverse channel arrangement, and their outcomes demonstrated that channel-to-rib widths of 2.8:0.5 and 4.2:0.3 achieve best performances for two layout respectively. Zeng et al. [24] adopted GA to investigate the optimal cross-sectional shape of trapezoidal channels in a PEMFC. The optimal design obtained a current density increase of 10.92% compared to the basic model. Liu et al. [25] separately optimized the operation condition and channel structure of a PEMFC by multi-objective GA taking into consideration of output power and power consumption.

According to the aforementioned researches, the performance of PEMFCs can be improved through elaborately designed and optimized channels based on mass transfer enhancement, presenting on some aspects as increasing reaction rate to improve current density as well as output power. However, due to the gas flow resistance, the progress is at the expense of an increase in pressure drop between the inlet and outlet of the channel, leading to an extra power consumption. Thus, pressure drop also has an important effect on the overall performance of PEMFCs [14,20,24–26]. Nowadays, bionic designs with low resistance characteristics attract abundant attention from researchers. A good review [27] summarized the bio-inspired ideas applied to the layout of flow field in PEMFCs, while applications in the channel shape is rarely found. Recently, inspired by the fins of cuttlefish, our group proposed a novel type of wave structure [28] whose amplitude gradually varies from the middle to the side, as shown in Fig. 1. This bio-inspired wave-like structure was demonstrated to be competitive in reducing flow resistance and improving the overall performance compared to the conventional wavy structures.

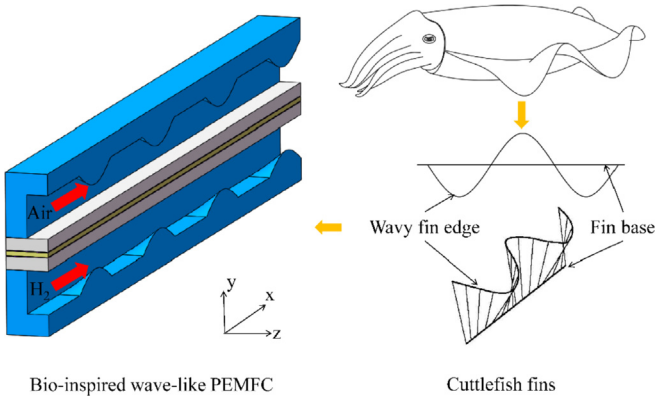

Fig. 1. Cuttlefish fins and bio-inspired wave-like PEMFC.

In this study, a three-dimensional model of PEMFC is established in COMSOL Multiphysics with a bio-inspired wave-like structure applied to the flow channel, as displayed in Fig. 1. The effect of this novel design on the overall performance is investigated, including the current density and pressure drop. Simultaneously, the result is compared with the basic straight channel model and conventional wave-like channel model. Further, two geometric parameters: center amplitude and number of wave cycles are automatically optimized using genetic algorithm via MATLAB combined with COMSOL to obtain the best waveform.

2. Design description

The geometrical schematic diagram of a single PEMFC with bio-inspired wave-like channels is presented in Fig. 2 and the geometrical and operating parameters are listed in Table 1. A PEMFC consists of anode/cathode bipolar plate (BP), anode/cathode channel, anode/cathode GDL, anode/cathode CL and membrane. The bio-inspired wave-like channel is illustrated at the top right of Fig. 2. The wavy blocks along the channel display as a sinusoidal shape and they are connected by straight path whose length is equal to the half wavelength (*E/2*). One straight path and one wavy block form a complete cycle, extending to the entire channel. From the cross-section of channel at the bottom right of Fig. 2, it is clear that the amplitude of the wave gradually increases from the two sides to the center of the channel, with zero at the both sides and maximum at the center. The number of wave cycles (*N*) along the channel and the center amplitude (*H*) are defined as variable geometric parameters.

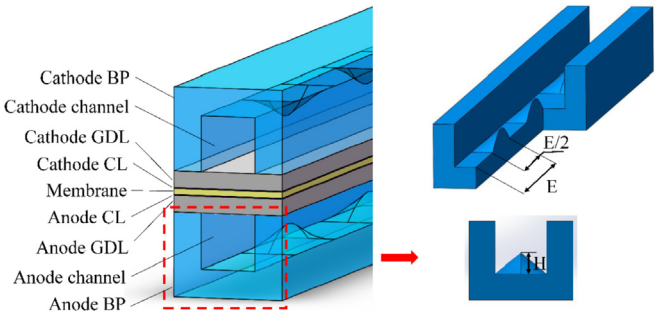

Fig. 2. Geometrical schematic diagram of a PEMFC with bio-inspired wave-like channel.

Table 1
Geometric and operating parameters [24,29–31].

Parameters (symbol)	Value	Unit
Channel length (L_{ch})	20	mm
Channel width (W_{ch})	1	mm
Channel height (H_{ch})	1	mm
Rib width (W_{rib})	1	mm
GDL thickness (H_{GDL})	0.3	mm
CL thickness (H_{CL})	1.29×10^{-2}	mm
Membrane thickness (H_{mem})	0.108	mm
GDL porosity (ε)	0.4	–
GDL permeability (K)	1.76×10^{-11}	m^2
Air stoichiometric flow ratio (ζ_c)	3	–
H_2 stoichiometric flow ratio (ζ_a)	3	–
Operating pressure (p)	1	atm
Operating temperature (T)	343.15	K
Relative humidity of inlet flows (RH)	100%	–
Anode reference exchange current density (j_a^{ref})	1.05×10^{10}	A/m^3
Cathode reference exchange current density (j_c^{ref})	100	A/m^3
Oxygen reference concentration ($C_{O_2}^{ref}$)	56.4	mol/m^3
Hydrogen reference concentration ($C_{H_2}^{ref}$)	3.39	mol/m^3
Reference diffusivity of H_2 in H_2O ($D_{H_2-H_2O}^{ref}$)	9.15×10^{-5}	m^2/s
Reference diffusivity of O_2 in H_2O ($D_{O_2-H_2O}^{ref}$)	2.82×10^{-5}	m^2/s
Reference diffusivity of O_2 in N_2 ($D_{O_2-N_2}^{ref}$)	2.2×10^{-5}	m^2/s
Reference diffusivity of H_2O in N_2 ($D_{H_2O-N_2}^{ref}$)	2.56×10^{-5}	m^2/s
Equivalent weight of electrolyte in membrane (EW)	1.1	kg/mol
Faraday's constant (F)	96487	C/mol
Universal gas constant (R)	8.314	J/mol K

3. Model development

3.1. Computational domain and model assumptions

A three-dimensional, single-phase, non-isothermal and steady-state PEMFC model is developed in order to evaluate the proposed channel design. To access the comprehensive influence of the bio-inspired wave-like channel on the overall performance of PEMFC, it is compared with the basic straight channel and conventional wave-like channel. As shown in Fig. 3, half of a single fuel cell with symmetric boundary condition is employed as the computational domain to save the computational recourse.

To simplify the model, the following assumptions are set: the gas mixtures are assumed to be ideal, and the gas flow in the channel is laminar; water inside the fuel cell is considered to be in vapor phase; the membrane is fully humidified and impermeable; GDLs and CLs are considered to be isotropic and homogenous.

3.2. Governing equations

The model established is described by the governing equations expressed as:

Continuity equation:

$$\nabla \cdot (\rho \mathbf{u}) = S_m \tag{1}$$

Momentum equation:

$$\nabla \cdot (\varepsilon \rho \mathbf{u}\mathbf{u}) = -\varepsilon \nabla p + \nabla \cdot \left(\varepsilon \mu_{eff} \nabla \mathbf{u}\right) + S_{mom} \tag{2}$$

Energy equation:

$$\rho C_p \mathbf{u} \cdot \nabla T = \nabla \cdot \left(k_{eff} \nabla T\right) + S_T \tag{3}$$

Species transport equation:

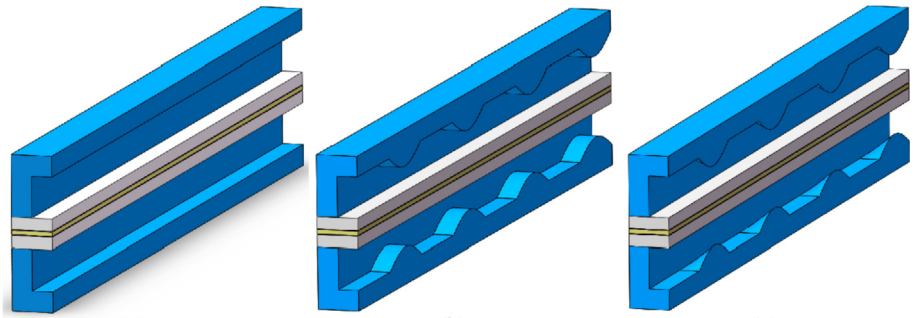

Fig. 3. Computational domain of PEMFCs with different channels.

$$\rho \mathbf{u} \cdot \nabla \omega_i = \nabla \cdot \left(\rho D_{ij}^{\text{eff}} \nabla \omega_i \right) + S_i \tag{4}$$

Charge conversation equation:

$$\nabla \cdot (\sigma_s \nabla \phi_s) + S_{\text{sol}} = 0 \tag{5}$$

$$\nabla \cdot (\sigma_m \nabla \phi_m) + S_{\text{mem}} = 0 \tag{6}$$

Water conservation equation in membrane:

$$\nabla \cdot (D_\lambda \nabla \lambda) + S_\lambda = 0 \tag{7}$$

The source terms in Eqs. (1)–(7) are dependent on different components or species, summarized in Table 2. D_{ij}^{eff} in Eq. (4) is effective species diffusivity, which can be described by the Bruggeman's equation. According to Berning et al. [31], it can be expressed as follows:

$$D_{ij}^{\text{eff}} = \varepsilon^{1.5} D_{ij}^{0}(T_0, P_0) \frac{P_0}{P} \left(\frac{T}{T_0} \right)^{1.5} \tag{8}$$

In Eq. (7), λ is the water content in the membrane, which can be described as a function of water activity a. Further, the electro-osmotic drag coefficient n_d, the water diffusivity D_λ and the proton conductivity σ_m are correlated with λ [32,33].

$$a = \frac{C_w RT}{P_{H_2O}^{\text{sat}}} \tag{9}$$

$$\lambda = \begin{cases} 0.043 + 17.8a - 39.85a^2 + 36.0a^3 & 0 < a \le 1 \\ 14 + 1.4(a-1) & 1 < a \le 3 \end{cases} \tag{10}$$

$$n_d = \frac{2.5\lambda}{22} \tag{11}$$

$$D_\lambda = \begin{cases} 3.1 \times 10^{-7} \frac{\rho_m}{EW} \lambda \left(e^{0.28\lambda} - 1 \right) \cdot e^{(-2346/T)} & 0 < \lambda \le 3 \\ 4.17 \times 10^{-8} \frac{\rho_m}{EW} \lambda (1 + 161 e^{-\lambda}) \cdot e^{(-2346/T)} & otherwise \end{cases} \tag{12}$$

$$\sigma_m = (0.5139\lambda - 0.326) \exp\left[1268 \left(\frac{1}{303} - \frac{1}{T} \right) \right] \tag{13}$$

In addition, a simplified agglomerate model is chosen to evaluate the electrochemical reaction within the catalyst layer. The reaction rates J_i can be determined by the Bulter-Volmer equation and an effectiveness coefficient η_{agg} is defined to modify the rates taking into consideration of the diffusion resistance [34,35]. The effective current density J_i^{eff} can be expressed as follows:

Table 2
Source terms in governing Eqs. (1)–(7).

Source terms	Expression	Components
Mass source term (S_m)	$S_m = -\frac{J_a^{\text{eff}}}{2F} M_{H_2} - \frac{n_d J_a^{\text{eff}}}{F} M_{H_2O}$	Anode CL
	$S_m = -\frac{J_c^{\text{eff}}}{4F} M_{O_2} + \frac{(1+2n_d) J_c^{\text{eff}}}{2F} M_{H_2O}$	Cathode CL
Momentum source term (S_{mom})	$S_{\text{mom}} = -\frac{\mu_{\text{eff}} \varepsilon^2}{K} \mathbf{u}$	GDL/CL
Energy source term (S_T)	$S_T = I^2 R_{\text{ohm}} + h_{\text{reaction}} + \eta R_{a,c}$	All
Species source term (S_i)	$S_{H_2} = -\frac{J_a^{\text{eff}}}{2F} M_{H_2}$	Anode CL
	$S_{O_2} = -\frac{J_c^{\text{eff}}}{4F} M_{O_2}$	Cathode CL
	$S_{H_2O} = \frac{J_c^{\text{eff}}}{2F} M_{H_2O}$	
Charge source term (S_{sol}, S_{mem})	$S_{\text{sol}} = -J_a$; $S_{\text{mem}} = J_a$	Anode CL
	$S_{\text{sol}} = J_c$; $S_{\text{mem}} = -J_c$	Cathode CL
Water content source term (S_λ)	$S_\lambda = -\nabla \cdot \left(\frac{n_d i}{F} \right)$	Membrane

$$J_i = J_i^{\mathrm{ref}} \left(\frac{C_k}{C_k^{\mathrm{ref}}}\right)^{\gamma_i} \left[\exp\left(\frac{\alpha_a F}{RT}\eta\right) - \exp\left(\frac{\alpha_c F}{RT}\eta\right)\right] \tag{14}$$

$$\eta_{\mathrm{agg}} = \frac{3}{\phi_{\mathrm{L}}}\left(\frac{1}{\tanh(\phi_{\mathrm{L}})} - \frac{1}{\phi_{\mathrm{L}}}\right) \tag{15}$$

$$\phi_{\mathrm{L}} = L_{\mathrm{agg}}\sqrt{\frac{|J_i|}{C_k D_k^{\mathrm{m}}}} \tag{16}$$

$$J_i^{\mathrm{eff}} = \eta_{\mathrm{agg}} J_i \tag{17}$$

where i can be a or c indicating anode and cathode, respectively. C_k is reactant concentration, where k can be hydrogen in anode or oxygen in cathode.

3.3. Boundary conditions

As mentioned before, the symmetric boundary conditions are employed in z direction of the model. Meanwhile, the no-flux conditions are applied to the external surface excluding the inlets and outlets of channels. The hydrogen and air flows with full humidity are supplied into the anode and cathode channels, respectively. The inlet temperatures T_{in} as well as the temperatures of surrounding walls are defined as operating temperature. The inlet species mass fraction ω_k^{in} can be determined from the inlet temperature, inlet pressure and inlet relative humidity according to the ideal gas law. Furthermore, the inlet velocities can be calculated as follows:

$$u_{\mathrm{a}}^{\mathrm{in}} = \zeta_{\mathrm{a}} \frac{i_{\max}}{2F} A_{\mathrm{m}} \frac{1}{\omega_{\mathrm{H_2}}^{\mathrm{in}}} \frac{RT_{\mathrm{a}}^{\mathrm{in}}}{p_{\mathrm{a}}^{\mathrm{in}}} \frac{1}{A_{\mathrm{ch}}} \tag{18}$$

$$u_{\mathrm{c}}^{\mathrm{in}} = \zeta_{\mathrm{c}} \frac{i_{\max}}{4F} A_{\mathrm{m}} \frac{1}{\omega_{\mathrm{O_2}}^{\mathrm{in}}} \frac{RT_{\mathrm{c}}^{\mathrm{in}}}{p_{\mathrm{c}}^{\mathrm{in}}} \frac{1}{A_{\mathrm{ch}}} \tag{19}$$

where $i_{\max}$ is the maximum average current density, A_{m} and A_{ch} are the geometrical area of the membrane and the cross-section area of the channel, respectively. The outlet pressures in both anode and cathode are prescribed as the operating pressure. The gradient for other variables in the channel direction is assumed to be zero.

3.4. Numerical implementation

The commercial software COMSOL Multiphysics 5.3 is chosen to perform the present investigation, using the finite volume method. These coupled governing equations are iteratively solved in segregated solvers. Four different sizes of grids with 34650, 46800, 57288 and 107712 hexahedron elements are conducted to test the mesh independence. As shown in Fig. 4, when the operating potential is 0.4 V, the relative error of current density between grid systems with 46800 and 107712 elements is limited within 0.06%. Therefore, the grid system with 46800 elements is dense enough and adopted for the subsequent simulations. The computational grids for PEMFC model with a bio-inspired wave-like channel is shown in Fig. 5. For diffusion layers, catalyst layers and membrane, they have small and different thicknesses thereby meshes are densified in varying degrees to improve the accuracy of calculation. It takes about 12 min to obtain one solution on an Intel Xeon 2.4 GHz workstation with a 32.0 RAM.

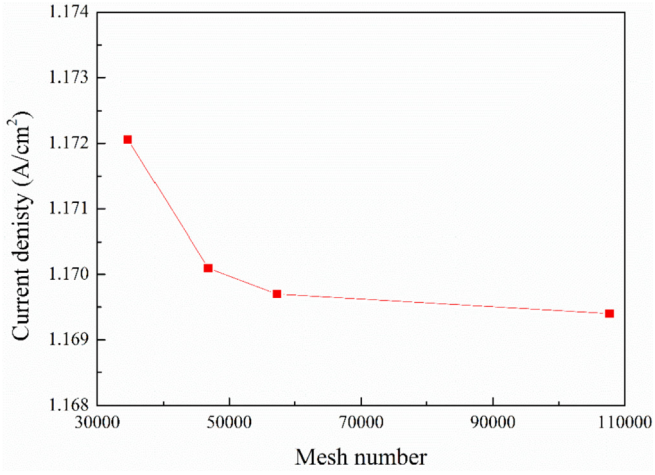

Fig. 4. Grid independent test.

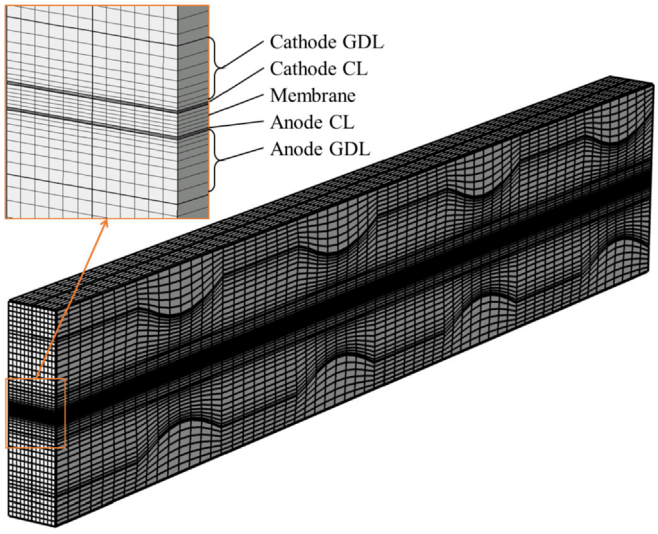

Fig. 5. Computational grids for PEMFC calculation.

3.5. Model validation

To ensure the accuracy of the numerical model, the polarization curve of a straight channel PEMFC obtained by simulation is compared with the experimental data of Wang et al. [29], as shown in Fig. 6. It can be observed that the simulation results are in good agreement with the experimental data and the difference is within 4.46% at high current density. Therefore, the model is validated to be reliable.

4. Results and discussion

4.1. Comparison of three types of channels

In this section, in order to evaluate the special effects of the bio-inspired wave-like channels on PEMFC performance, a comprehensive comparison of three different types of channel is performed based on the current density and cathode pressure drop between inlet and outlet. The influences of the number of wave cycles and the center amplitude are also investigated. Further, the mass transfer enhancement mechanism is discussed based on the velocity field and reactants concentration distribution.

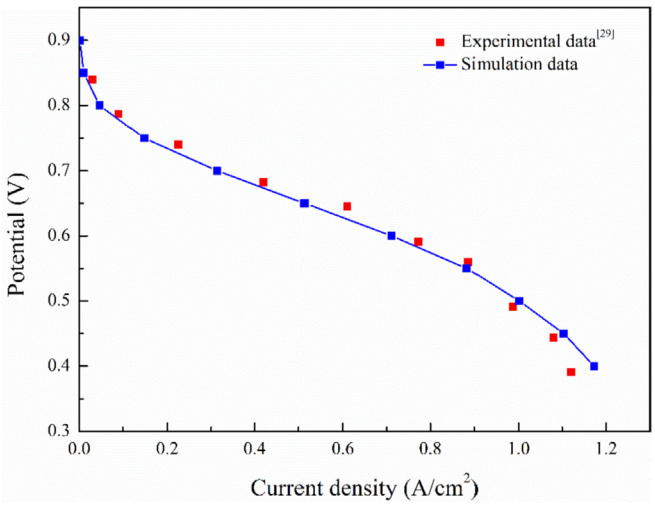

Fig. 6. Model validation: comparison of polarization curve between simulation and experiment for a straight channel PEMFC.

Fig. 7 illustrates the current density and pressure drop of PEMFCs with three different channels at the potential of 0.4 V. Here, only cathode pressure drop is considered. It can be observed that both PEMFC with conventional wave-like channel and bio-inspired wave-like channel cause a significant increase on the current density compared to the PEMFC with a basic straight channel in all simulation cases, and they also lead to a higher pressure drop. However, the difference is that the conventional wave-like structure achieves a high current density increase at the cost of a much higher pressure drop. Relatively, the bio-inspired wave-like structure obtains a moderate current density increase with only a slight pressure drop increase.

Generally speaking, if the center amplitude is too small, the impact of wavy blocks on the gas flow in the channel is not obvious. Whereas if the center amplitude is too large, the physical obstruction caused by the wavy blocks will lead to significant flow resistance and excessive power consumption, which is not worthy. In our case, considering the total height of the channel is 1 mm, an arithmetic progression with tolerance of 0.1 mm in a moderate range, which are 0.2, 0.3, 0.4, 0.5, 0.6 and 0.7 mm, is chosen as variables to investigate the effect of different H on the performance

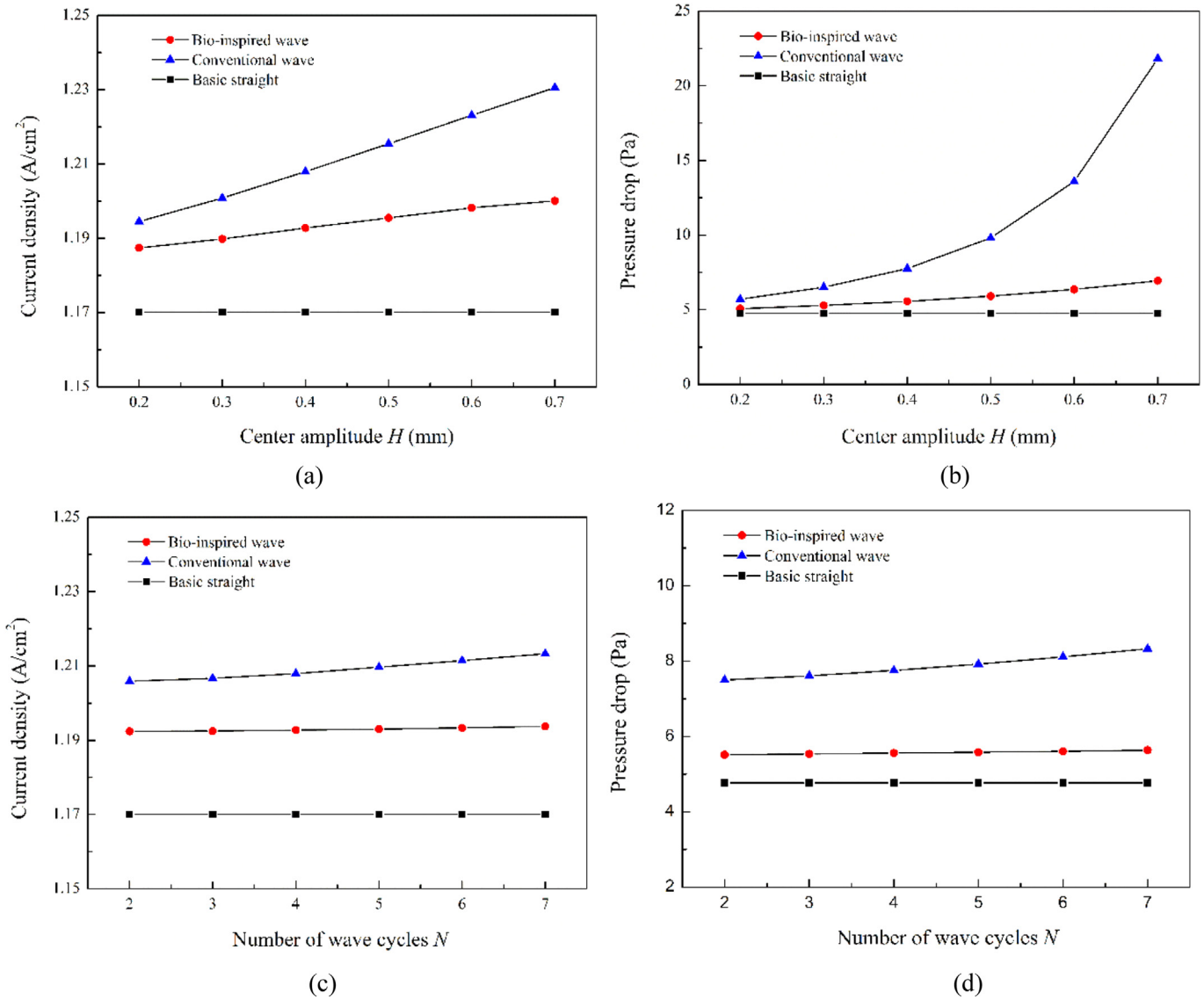

Fig. 7. PEMFC performance comparison of three different channels at $V_{cell} = 0.4$ V: (a) effect of center amplitude on current density ($N = 4$), (b) effect of center amplitude on cathode pressure drop ($N = 4$), (c) effect of number of wave cycles on current density ($H = 0.4$ mm), (d) effect of number of wave cycles on cathode pressure drop ($H = 0.4$ mm).

Table 3
PEMFC performance comparison of three types of channels at $V_{cell} = 0.4$ V ($H = 0.7$ mm, $N = 7$).

Channel types	Current density (A/cm^2)	Pressure drop (Pa)
Basic straight channel	1.170	4.766
Conventional wave-like channel	1.242	26.143
Bio-inspired wave-like channel	1.204	7.207

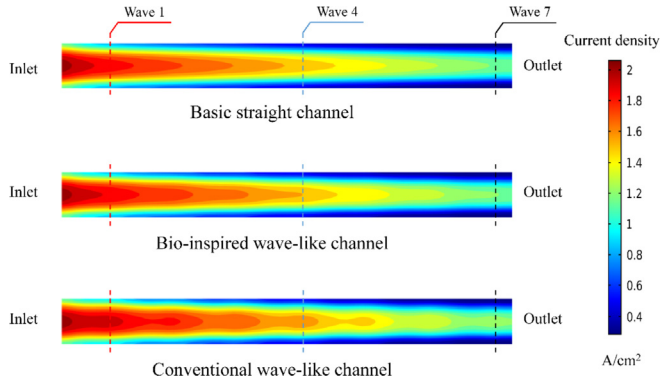

Fig. 8. Current density distribution in the membrane at $V_{cell} = 0.4$ V ($H = 0.7$ mm, $N = 7$).

of PEMFC, as presented in Fig. 7 (a) and (b). A similar feature can be noticed that both the current density and pressure drop of two wave-like PEMFCs are increased as the center amplitude increases. However, it is apparent that the growth trend of PEMFC with conventional wave-like channels is much faster than the bio-inspired PEMFC, especially on the pressure drop, which means a remarkable extra power consuming. In other word, the bio-inspired PEMFC has an obvious advantage in stabilizing and controlling pressure drop growth while increasing the current density.

Fig. 7. (c) and (d) indicate the influence of the number of wave cycles N on the performance of PEMFC. Similarly, in order to balance the effect of wavy blocks on air flow and the resulting resistance, the number of wave cycles should be appropriate. Hence, the different N are selected as 2, 3, 4, 5, 6 and 7 in this study. The consequent is similar to what the center amplitude provides, but the effect of the number of wave cycles is relatively less profound. This result can be explained by the fact that the reactants are depleted continuously along the channel and most of them are consumed during the first one or two wavy cycles so that the concentration decreases quickly. The closer to the outlet, the lower reactant concentration. Although more wavy blocks are added behind, the influence is not evident. Together these results provide important insights that this bio-inspired wave-like channel can not only significantly improve the current density of PEMFC compared to the basic straight channel, but also evidently decrease the pressure drop of PEMFC compared to the conventional wave-like channel.

In Table 3, the values of PEMFC performance for the three types of channels are listed with $H = 0.7$ mm and $N = 7$ at a cell voltage of 0.4 V. What is striking about the figures is that compared to the basic straight channel, the conventional wave-like channel improves the current density by 6.15% and increases the pressure drop by 4.49 times, while the bio-inspired wave-like channel improves the current density by 2.91% and only increases the pressure drop by 0.51 times.

Fig. 8 illustrates the current density distribution in the membrane for PEMFCs with three different channels. It is apparent that the maximum current density is found at the inlet of the channel because of the highest reactants concentration at the beginning. As the reactants are gradually consumed along the flow channel, the current density decreases from the inlet to the outlet. Meanwhile, the current density is higher in the center of the channel than it under the ribs. Moreover, compared to the basic straight channel, both the bio-inspired wave-like channel and the conventional wave-like channel lead to a higher and more uniform current density distribution due to the periodical wavy protuberances. Closer inspection of the figure shows that there are seven periodic

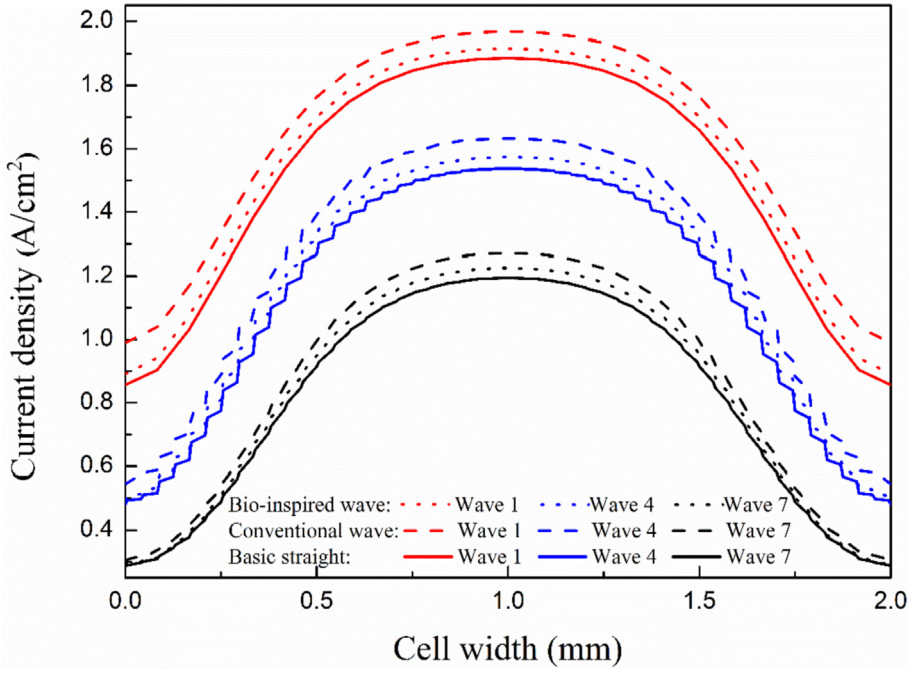

Fig. 9. Current density on three cut lines along the cell width at $V_{cell} = 0.4$ V ($H = 0.7$ mm, $N = 7$).

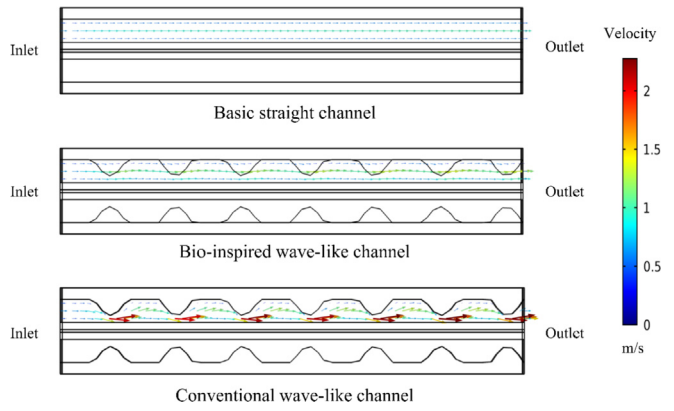

Fig. 10. Velocity vectors in cathode gas flow channel at $V_{cell} = 0.4$ V ($H = 0.7$ mm, $N = 7$).

enhancement regions, the quantity of which is exactly equal to the number of wave cycles.

In order to observe this phenomenon more directly, as shown Fig. 8, three cut lines along the cell width are selected, corresponding to the position of peaks of the first, fourth and seventh wavy blocks, respectively, the current densities of which are displayed in Fig. 9. Current density distributions for three types of channel along the cell width are all parabolic. The highest current density achieves on the wave 1 cut line near the inlet, followed by the wave 4 cut line, and the current density on the wave 7 cut line near the outlet is the minimum. It can be observed that the current density of both bio-inspired wave-like PEMFC and conventional wave-like PEMFC are higher than the basic straight PEMFC. Therefore, it confirms that both the bio-inspired wavy shape and the conventional wavy shape can effectively improve and unify the current density and the former has a more gentle effect than the later.

Gas supplied in the anode is pure hydrogen while it is air only involving 21% of oxygen by volume in the cathode. Besides, the flow resistance in the anode is much lower than that in the cathode due to the higher diffusion coefficient of hydrogen comparing to oxygen. Hence, the flow filed in the cathode is more important. To further analyze the mechanism of the performances improvement caused by the wave-like channels, the velocity vectors in cathode gas flow channel are evaluated as shown in Fig. 10. In the basic straight channel, flow transport is smooth without obstructs. While in the two wave-like channels, wavy blocks gradually reduce the flow area along the horizontal direction forming a constricted channel. Consequently, the flow of species is pressed under the wavy blocks so that the flow is accelerated. Furthermore, due to the blocks, the flow is forced to change the direction, thereby an evident vertical velocity component occurs in the two wave-like channels. Since this vertical velocity component is in the same direction of the concentration gradient, according to the field synergy principle to the process of convective mass transfer, it can divert more reactants to the GDL, enhancing the mass transfer process. More reactants have access to the catalyst layer, leading to the electrochemical reaction accelerated and the efficiency increased.

Fig. 11 shows the oxygen molar concentration on the center line of the interface between cathode gas diffusion layer and catalyst layer, which is in harmony with the current density distribution in Fig. 8. It can be observed that the oxygen molar concentration decreases along the gas flow direction in the basic case as the reactants are consumed for reaction, and the rate of decrease gradually slows down. While the two wave-like channels can both increase the oxygen molar concentration in fluctuation. There are seven peaks due to the forced convection caused by the wavy blocks correspond to the seven current density enhancement regions in Fig. 8. Furthermore, the larger the center amplitude, the larger the peak value. This phenomenon is attributable to the vertical velocity in Fig. 10 forcing the gases into the CL, further verifying the effect of the wave-like channels on mass transfer

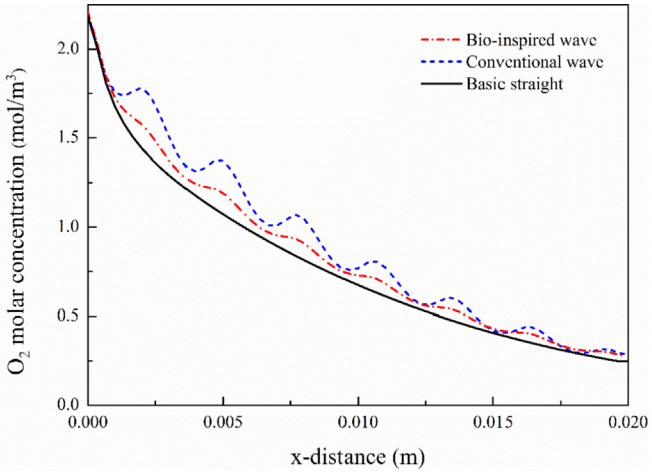

Fig. 11. Oxygen molar concentration on the center line of the interface between cathode GDL and CL at $V_{cell} = 0.4$ V ($H = 0.7$ mm, $N = 7$).

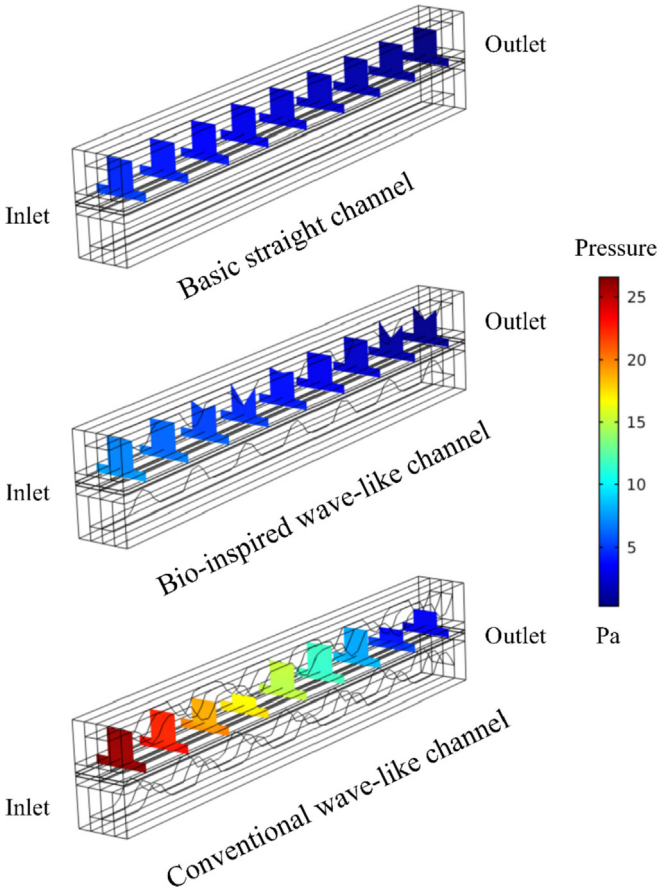

Fig. 12. Cathode pressure drop at 0.4 V ($H = 0.7$ mm, $N = 7$).

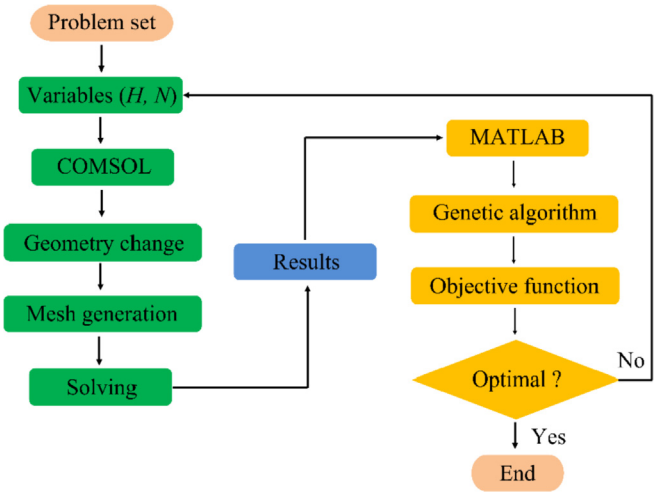

Fig. 13. Flow chart of the optimization process.

enhancement. In addition, along the channel, the oxygen molar concentration of two wave-like channels is higher than the straight channel whether at the peaks or valleys. The average oxygen molar concentration of the basic straight channel, bio-inspired wave-like channel and the conventional wave-like channel at the interface is 0.402, 0.424 and 0.469 mol/m^3, respectively.

Turning now to the evidence on cathode pressure drop for PEMFCs with three different channels, displayed in Fig. 12. It is observed that the conventional wave-like channel leads to an astonishing pressure drop. However, only a slight increase of pressure drop is caused by the bio-inspired wave-like channel. As the amplitude gradually increases from the ribs to the center of the channel, the interference with the gas flow gently increases. It can intensely push the fluid in the center region into GDL while reserving sufficient space on the two sides. As a result, only the mass transfer in the center region is enhanced whereas the flow on the two sides with greater frictional resistance hardly changes. Hence, the disturbance caused by bio-inspired wave-like channel is not as strong as that by the conventional wave-like channel so that the flow resistances in the former is much lower than the later.

4.2. Optimization of bio-inspired wave-like channel

According to the simulation results above, the current density and pressure drop simultaneously increase as center amplitude and number of wave cycles increase. In this section, by using the genetic algorithm to optimize the two variables, the best waveform of the bio-inspired wave-like channel is captured to ensure that the current density is as large as possible and the pressure drop is as small as possible. MATLAB is selected to implement the combination of GA and COMSOL [23–25]. This approach can automatically generate new variables, update numerical simulation and check the optimality, as shown in Fig. 13.

For a PEMFC, the output power E_{cell} and the power consumption of flow E_{con} can be expressed as follows:

$$E_{cell} = V_{cell} i_{ave} A_m \tag{20}$$

$$E_{con} = \Delta p_c u_c^{in} A_{ch}^{in} \tag{21}$$

In Eq. (20), V_{cell}, i_{ave}, and A_m represent the fuel cell operational voltage, average current density and activated area, respectively. In Eq. (21), p_c, u_c^{in} and A_{ch}^{in} are the cathode pressure drop, inlet velocity

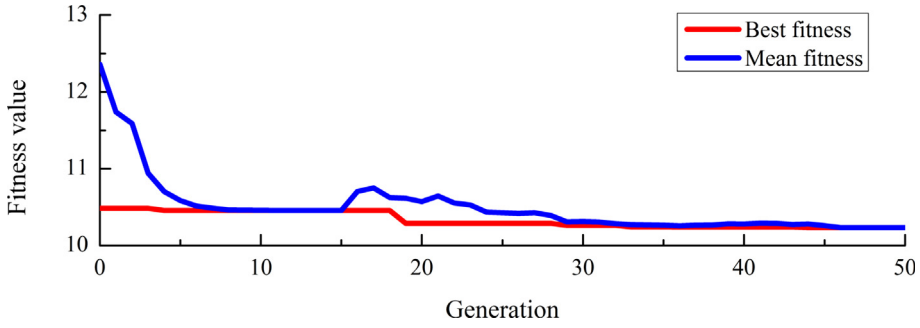

Fig. 14. Optimization results.

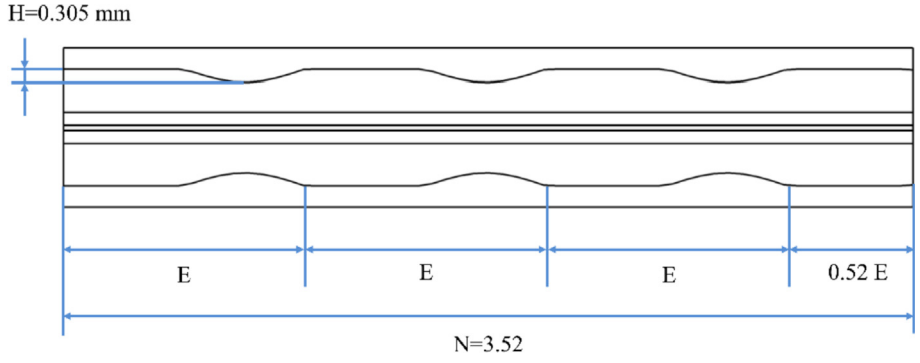

Fig. 15. Longitudinal section view of optimal design.

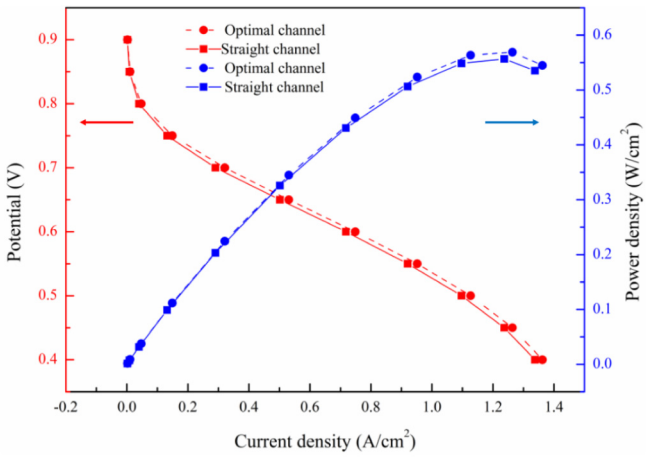

(a)

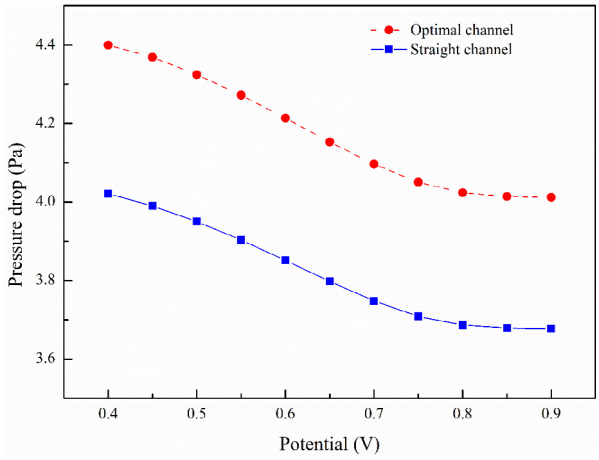

(b)

Fig. 16. PEMFC performances comparison between the optimal channel and straight channel: (a) polarization curve and output power, (b) cathode pressure drop.

and inlet cross-sectional area of channel.

In this study, the objective function is defined as [10,24]:

$$f = k\frac{E_{con}}{E_{cell}} \tag{22}$$

where k is a constant equal to 1e6. The overall performance of PEMFC reaches optimal as the objective function gets the minimum value.

In addition, the following constrains are imposed on the two variables:

$0.3\ \text{mm} \le H \le 0.6\ \text{mm}$

$3 \le N \le 6$

During the optimization process, other parameters are constant. The operational voltage is set as 0.4 V. The channel width is set as 1.2 mm and the rib width is set as 0.8 mm since properly increasing the channel width can provide a better gas supply and a larger contact area with GDL [36]. In this study, as only two variables are investigated, a population size of 20 and a generation number of 50 are selected for the genetic algorithm to keep the calculation accuracy and save the computation time. It takes about approximately 9 days to obtain the final optimization results on an Intel Xeon 2.4 GHz workstation with a 32.0 RAM.

After 50 generation evolutions, the optimization results are obtained, as presented in Fig. 14. The results converge after the 45th generation at which the mean fitness value and the best fitness value are identical. The best fitness value is 10.2322, corresponded to the center amplitude H and number of wave cycles N of 0.305 mm and 3.52, respectively. The longitudinal section shape of PEMFC with the optimal bio-inspired wave-like channel is shown in Fig. 15. There are three wavy blocks and the gas species flow in and out both along a straight channel which can minimize the resistance.

Fig. 16 presents the performances of PEMFCs with optimal bio-inspired wave-like channel and with basic straight channel. It can be observed that the optimal case generates a higher current density so that the output power increases, compared to the basic case. The maximum output density obtains at the potential of 0.45 V with an increment of 2.2%. Moreover, the optimal case brings a higher cathode pressure drop as expected and the discrepancy between the two cases is almost constant at 0.38 Pa at different potentials.

5. Conclusion

A bio-inspired wave-like channel for PEMFCs was designed in this study. The performance of PEMFCs with this bio-inspired wave-like channel was studied by three-dimensional numerical simulations under different center amplitude and number of wave cycles. The result is compared with PEMFCs with a basic straight channel and a conventional wave-like channel. Subsequently, the optimal waveform of bio-inspired wave-like channel was investigated by genetic algorithm. The simulation result and discussion indicate the following conclusions:

1. Increasing the center amplitude and the number of wave cycles can lead to simultaneous increase of current density and pressure drop, and the effect of the center amplitude is relatively more significant than the number of wave cycles.
2. Comparing to the basic straight channel, the bio-inspired wave-like channel can change the magnitude and direction of the gas velocity because of the physical obstruction caused by wavy blocks, so that more reactants in the center region of the channel can diffuse into the GDL. As a result, fuel utilization improves and the current density increases.
3. Comparing to the conventional wave-like channel, the bio-inspired wave-like channel reserves the flow area on the two sides of the channel so that the flow resistance is lower, significantly reducing the pressure drop.
4. The best performance obtained when the center amplitude and the number of wave cycles were 0.305 mm and 3.52, respectively. At the potential of 0.45 V, the output power density of the optimal case is 2.2% greater than that of the basic case.

Declaration of competing interest

The authors claim that none of the material in the paper has been published or is under consideration for publication elsewhere.

Acknowledgments

The work was supported by the National Natural Science Foundation of China (Grant No. 51776079 & 51376004), and the National Key Research and Development Program of China (Grant

No. 2017YFB0603501-3).

References

[1] Wilberforce T, Alaswad A, Palumbo A, Dassisti M, Olabi AG. Advances in stationary and portable fuel cell applications. Int J Hydrogen Energy 2016;41(37):16509–22.
[2] Wang Y, Chen KS, Mishler J, Cho SC, Adroher XC. A review of polymer electrolyte membrane fuel cells: technology, applications, and needs on fundamental research. Appl Energy 2011;88(4):981–1007.
[3] Raj A, Shamim T. Investigation of the effect of multidimensionality in PEM fuel cells. Energy Convers Manag 2014;86:443–52.
[4] Siegel C. Review of computational heat and mass transfer modeling in polymer-electrolyte-membrane (PEM) fuel cells. Energy 2008;33(9):1331–52.
[5] Abdul Rasheed RK, Liao Q, Caizhi Z, Chan SH. A review on modelling of high temperature proton exchange membrane fuel cells (HT-PEMFCs). Int J Hydrogen Energy 2017;42(5):3142–65.
[6] Wu H-W. A review of recent development: transport and performance modeling of PEM fuel cells. Appl Energy 2016;165:81–106.
[7] Ramin F, Sadeghifar H, Torkavannejad A. Flow field plates with trap-shape channels to enhance power density of polymer electrolyte membrane fuel cells. Int J Heat Mass Transf 2019;129:1151–60.
[8] Yin Y, Wang X, Shangguan X, Zhang J, Qin Y. Numerical investigation on the characteristics of mass transport and performance of PEMFC with baffle plates installed in the flow channel. Int J Hydrogen Energy 2018;43(16):8048–62.
[9] Fan L, Niu Z, Zhang G, Jiao K. Optimization design of the cathode flow channel for proton exchange membrane fuel cells. Energy Convers Manag 2018;171:1813–21.
[10] Shen J, Tu Z, Chan SH. Enhancement of mass transfer in a proton exchange membrane fuel cell with blockage in the flow channel. Appl Therm Eng 2019;149:1408–18.
[11] Mancusi E, Fontana É, Ulson de Souza AA, Guelli Ulson de Souza SMA. Numerical study of two-phase flow patterns in the gas channel of PEM fuel cells with tapered flow field design. Int J Hydrogen Energy 2014;39(5):2261–73.
[12] Heidary H, Kermani MJ, Dabir B. Influences of bipolar plate channel blockages on PEM fuel cell performances. Energy Convers Manag 2016;124:51–60.
[13] Li W, Zhang Q, Wang C, Yan X, Shen S, Xia G, Zhu F, Zhang J. Experimental and numerical analysis of a three-dimensional flow field for PEMFCs. Appl Energy 2017;195:278–88.
[14] Chowdhury MZ, Genc O, Toros S. Numerical optimization of channel to land width ratio for PEM fuel cell. Int J Hydrogen Energy 2018;43(23):10798–809.
[15] Randrianarizafy B, Schott P, Chandesris M, Gerard M, Bultel Y. Design optimization of rib/channel patterns in a PEMFC through performance heterogeneities modelling. Int J Hydrogen Energy 2018;43(18):8907–26.
[16] Jeon DH. Effect of channel-rib width on water transport behavior in gas diffusion layer of polymer electrolyte membrane fuel cells. J Power Sources 2019;423:280–9.
[17] Jia X, Zhang H, Zheng Q. Numerical investigation on the effect of hot running rim seal clearance on hot gas ingestion into rotor-stator system. Appl Therm Eng 2019;152:79–91.
[18] Ge Y, Wang S, Liu Z, Liu W. Optimal shape design of a minichannel heat sink applying multi-objective optimization algorithm and three-dimensional numerical method. Appl Therm Eng 2019;148:120–8.
[19] Behrou R, Pizzolato A, Forner-Cuenca A. Topology optimization as a powerful tool to design advanced PEMFCs flow fields. Int J Heat Mass Transf 2019;135:72–92.
[20] Barati S, Khoshandam B, Ghazi MM. An investigation of channel blockage effects on hydrogen mass transfer in a proton exchange membrane fuel cell with various geometries and optimization by response surface methodology. Int J Hydrogen Energy 2018;43(48):21928–39.
[21] Seyhan M, Akansu YE, Murat M, Korkmaz Y, Akansu SO. Performance prediction of PEM fuel cell with wavy serpentine flow channel by using artificial neural network. Int J Hydrogen Energy 2017;42(40):25619–29.
[22] Tahmasbi AA, Hoseini A, Roshandel R. A new approach to multi-objective optimisation method in PEM fuel cell. Int J Sustain Energy 2015;34(5):283–97.
[23] Yang W-J, Wang H-Y, Lee D-H, Kim Y-B. Channel geometry optimization of a polymer electrolyte membrane fuel cell using genetic algorithm. Appl Energy 2015;146:1–10.
[24] Zeng X, Ge Y, Shen J, Zeng L, Liu Z, Liu W. The optimization of channels for a proton exchange membrane fuel cell applying genetic algorithm. Int J Heat Mass Transf 2017;105:81–9.
[25] Liu Z, Zeng X, Ge Y, Shen J, Liu W. Multi-objective optimization of operating conditions and channel structure for a proton exchange membrane fuel cell. Int J Heat Mass Transf 2017;111:289–98.
[26] Wilberforce T, El-Hassan Z, Khatib FN, Al Makky A, Mooney J, Barouaji A, Carton JG, Olabi A-G. Development of Bi-polar plate design of PEM fuel cell using CFD techniques. Int J Hydrogen Energy 2017;42(40):25663–85.
[27] Arvay A, French J, Wang JC, Peng XH, Kannan AM. Nature inspired flow field designs for proton exchange membrane fuel cell. Int J Hydrogen Energy 2013;38(9):3717–26.
[28] Liang Y, Liu P, Zheng N, Shan F, Liu Z, Liu W. Numerical investigation of heat transfer and flow characteristics of laminar flow in a tube with center-tapered wavy-tape insert. Appl Therm Eng 2019;148:557–67.
[29] Wang L, Husar A, Zhou T, Liu H. A parametric study of PEM fuel cell performances. Int J Hydrogen Energy 2003;28(11):1263–72.
[30] Tao WQ, Min CH, Liu XL, He YL, Yin BH, Jiang W. Parameter sensitivity examination and discussion of PEM fuel cell simulation model validation: Part I. Current status of modeling research and model development. J Power Sources 2006;160(1):359–73.
[31] Berning T, Lu DM, Djilali N. Three-dimensional computational analysis of transport phenomena in a PEM fuel cell. J Power Sources 2002;106(1):284–94.
[32] Ju H, Meng H, Wang C-Y. A single-phase, non-isothermal model for PEM fuel cells. Int J Heat Mass Transf 2005;48(7):1303–15.
[33] Meng H. A three-dimensional PEM fuel cell model with consistent treatment of water transport in MEA. J Power Sources 2006;162(1):426–35.
[34] Siegel NP, Ellis MW, Nelson DJ, von Spakovsky MR. Single domain PEMFC model based on agglomerate catalyst geometry. J Power Sources 2003;115(1):81–9.
[35] Rismanchi B, Akbari MH. Performance prediction of proton exchange membrane fuel cells using a three-dimensional model. Int J Hydrogen Energy 2008;33(1):439–48.
[36] Yoon Y-G, Lee W-Y, Park G-G, Yang T-H, Kim C-S. Effects of channel and rib widths of flow field plates on the performance of a PEMFC. Int J Hydrogen Energy 2005;30(12):1363–6.